PLOS ONE

RESEARCH ARTICLE

Overproduction of Sch9 leads to its aggregation and cell elongation in *Saccharomyces cerevisiae*

Polina Drozdova[1¤a]*, Polina Lipaeva[1¤b], Tatyana Rogoza[1,2], Galina Zhouravleva[1,3], Stanislav Bondarev[1,3]*

1 Dept. of Genetics and Biotechnology, Saint Petersburg State University, St. Petersburg, Russia, **2** Vavilov Institute of General Genetics, St. Petersburg Branch, Russian Academy of Sciences, St. Petersburg, Russia, **3** The Laboratory of Amyloid Biology, Saint Petersburg State University, St. Petersburg, Russia

¤a Current address: Institute of Biology at Irkutsk State University, Irkutsk, Russia
¤b Current address: LLC "Innova Plus", St. Petersburg, Russia
* drozdovapb@gmail.com, p.drozdova@spbu.ru (PD); stanislavspbgu@gmail.com, s.bondarev@spbu.ru (SB)

Citation: Drozdova P, Lipaeva P, Rogoza T, Zhouravleva G, Bondarev S (2018) Overproduction of Sch9 leads to its aggregation and cell elongation in *Saccharomyces cerevisiae*. PLoS ONE 13(3): e0193726. https://doi.org/10.1371/journal.pone.0193726

Editor: Michael Polymenis, Texas A&M University College Station, UNITED STATES

Received: December 18, 2017

Accepted: February 16, 2018

Published: March 1, 2018

Data Availability Statement: All relevant data are within the paper and its Supporting Information files.

Funding: The investigation of Sch9 aggregation and corresponding bioinformatic analysis was supported by Russian Science Foundation (rscf.ru) grant 17-74-10159, while the study of effects of Sch9 overproduction on cell morphology was supported by RFBR (rfbr.ru) grant 16-04-00202. The funders had no role in study design, data

Abstract

The Sch9 kinase of *Saccharomyces cerevisiae* is one of the major TOR pathway effectors and regulates diverse processes in the cell. Sch9 belongs to the AGC kinase family. In human, amplification of AGC kinase genes is connected with cancer. However, not much is known about the effects of Sch9 overproduction in yeast cells. To fill this gap, we developed a model system to monitor subcellular location and aggregation state of overproduced Sch9 or its regions fused to a fluorescent protein. With this system, we showed that Sch9-YFP forms detergent-resistant aggregates, and multiple protein regions are responsible for this. This finding corroborated the fact that Sch9-YFP is visualized as various fluorescent foci. In addition, we found that Sch9 overproduction caused cell elongation, and this effect was determined by its C-terminal region containing kinase domains. The constructs we present can be exploited to create superior yeast-based model systems to study processes behind kinase overproduction in cancers.

Introduction

The Sch9 kinase of *Saccharomyces cerevisiae* has a plethora of functions. Sch9 is one of the major TOR effectors [1]. It takes part in regulation of protein synthesis in response to nutrient availability [1] and cell cycle progression [2]. Sch9 is also linked to such important processes as aging (as deletion of *SCH9* promotes longevity [3]) and maintenance of genome stability (as stable tetraploid clonal populations were characterized by increased Sch9 activity [4]). Strains deleted for *SCH9* are characterized by overall growth defect, which is expressed as significantly decreased cell size and growth rate [5]. However, such strains possess increased thermotolerance, chronological [3] and replicative [6] lifespan. This effect may be explained by constitutively active oxidative stress response system [7] preventing accumulation of age-related

collection and analysis, decision to publish, or preparation of the manuscript.

Competing interests: The authors have declared that no competing interests exist.

mutations [8], perturbed sphingolipid levels [9] or, more likely, a combined effect of these factors.

Sch9 belongs to the AGC kinase family [10]. The AGC (the abbreviation stands for protein kinases A, G and C) kinases are widespread in eukaryotes including both the animal and fungal kingdoms [11]. In *S. cerevisiae* the AGC group contains 17 members, which the Ypk1 and Ypk2 are the closest relatives to Sch9 [10]. Together, the corresponding genes form a co-orthologous group to PKB/SGK kinase genes in mammals, and all members of this group arise from several consequent duplications of a single sequence in the fungal and animal ancestor [12]. In mammals, the PKB and SGK kinases together with RSK and S6K comprise a subfamily of AGC kinases, activated by phosphorylation, members of which are implicated in different diseases including cancer [11]. RSK2 gene overexpression was detected in skin cancer tissues [13]. Amplifications of genome fragments increasing production of PKB/AKT kinases were found in carcinomas of the stomach, ovary, pancreas, and breast [14]. Some data were received about the role of SGK kinase activation in cancer [15, 16], however, S6K is the most extensively studied AGC member. Mammals contain two homologous S6Ks, S6K1 and S6K2, functions of which overlap only partially [17, 18]. The chromosomal region including the gene for S6K1 is amplified in different breast cancer cell lines and in 10-30% of primary tumors [19–21] and was determined as prognostic of metastatic capacity of human breast cancer [22]. At the same time, overexpression of either S6K1 or S6K2 correlates with worse prognosis in breast cancer [23]. Taken together, these data show that protein kinases of the AGC family constitute an important target for cancer therapy, and thus studies in the yeast model might provide important insight into the mechanisms of their functioning.

Although *SCH9* encodes one of the best studied AGC kinases in yeast, the effects of its overexpression have not been studied in detail. Overexpression of *SCH9* is neither lethal nor significantly toxic for the yeast cell [2], even though it causes heat sensitivity [24] and slightly increases the rate of age-dependent mutations [8]. However, evidence on Sch9 overproduction effects is scarce and does not significantly extend beyond the phenotypes listed above.

Results

Sch9-YFP is functional and not toxic when overproduced

To study effects of *SCH9* overexpression and localization of the corresponding protein we made a plasmid construct for production of Sch9 fused with YFP, under control of strong constitutive GPD (*TDH3*) promoter (p426GPD-SCH9YFP). The control construct (p426GPD-YFP) was identical to the experimental one but did not contain the *SCH9* gene sequence. Then we transformed a wild-type strain (BY4742) and a similar strain deleted for *SCH9* (*sch9Δ*-BY4741) with these constructs and confirmed that full-length Sch9-YFP was produced in both cases (S1A Fig). Moreover, we tested whether the overproduced protein could be phosphorylated and found that at least a fraction of Sch9-YFP had phosphorylated Thr^{737} residue; importantly, Sch9-YFP overproduction did not abolish phosphorylation of the native (genome-encoded) Sch9 (S1B Fig). *SCH9-YFP* overexpression was not toxic in either strain (S1C Fig), which corresponds well to the known data [2]. Interestingly, *sch9Δ*-BY4741 colonies overproducing *SCH9* still did not grow as well as the *SCH9* BY4742 colonies (S1C Fig). It means that these strains have growth differences, and thereafter will only be compared to the corresponding internal control. We also observed that *SCH9* overexpression caused elongation of cells (Fig 1); this fact will be described in detail below.

To check whether the C-terminal YFP tag disturbs functioning of Sch9, we transformed the strain deleted for *SCH9* with a centromeric plasmid bearing *SCH9* driven by its own promoter, analogous construct with *SCH9-YFP* and the corresponding empty vector. Then we compared

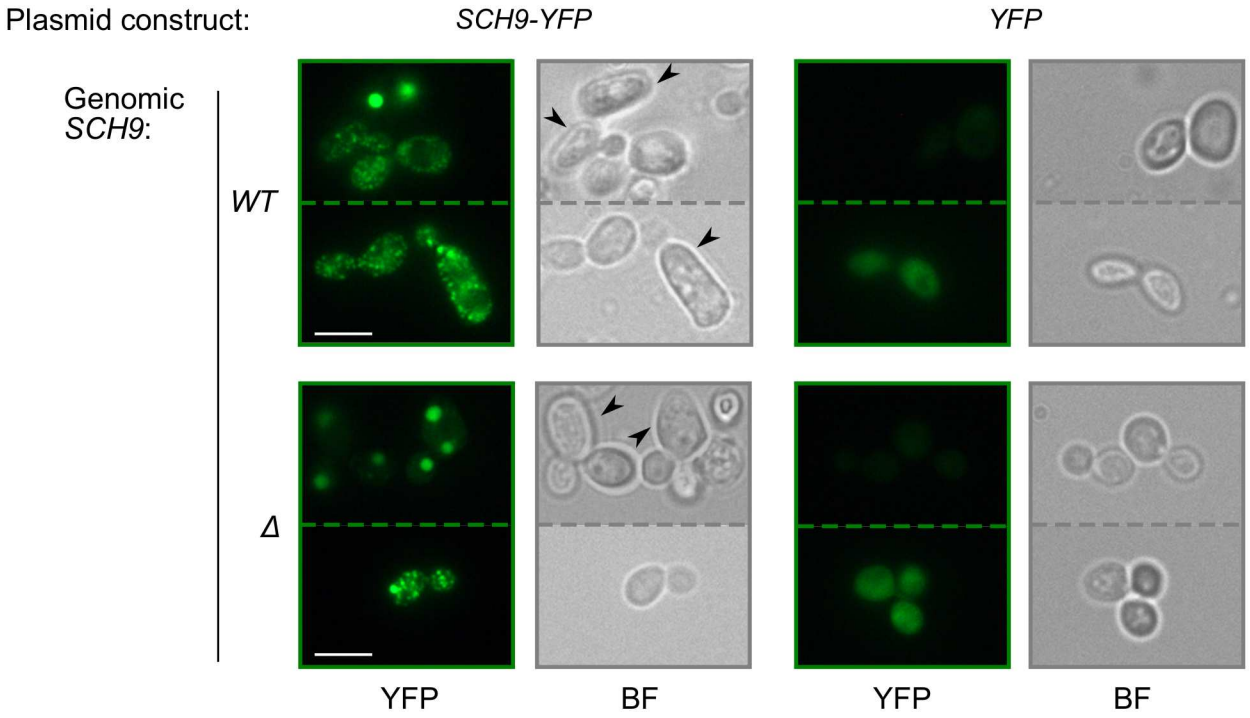

Fig 1. Overproduced Sch9-YFP forms distinct fluorescent foci. Scale bar indicates 5 μm. BF, bright-field microscopy. Dashed lines separated different fields of view. *WT* and *Δ* designate BY4742 and *sch9Δ*-BY4741 strains, respectively. Arrowheads mark elongated cells.

https://doi.org/10.1371/journal.pone.0193726.g001

growth of the transformants on medium containing galactose and raffinose as carbon sources (S1D Fig), as *SCH9* deletion had been found to impede growth on galactose/raffinose-containing media [1]. Indeed, we found that cells with *SCH9* grew better on this medium than the empty vector control (S1D Fig, compare lanes 1 and 2 on galactose/raffinose medium). Importantly, the Sch9-YFP construct was indistinguishable from the one with untagged Sch9 (compare lanes 2 and 3). These data suggest that the YFP tag does not interfere with normal Sch9 functioning.

In addition, we tested whether overproduced Sch9-YFP compensated for this galactose utilization defect and found that it acted in the same way as single-copy *SCH9-YFP*, *i. e.* improved growth on galactose/raffinose-containing medium. Interestingly, we also noticed that the strains overproducing Sch9-YFP grew slower on SC-Ura, as after three days of incubation they formed smaller colonies, but after six days there was almost no difference (S1D Fig). Thus, overproduced Sch9-YFP is at least partially functional (it can be phosphorylated and compensates for the growth defect of the *SCH9*-deleted strain); it is not toxic but decreases cell division rate.

Overproduced Sch9-YFP forms fluorescent foci and SDS-resistant aggregates

The Sch9-YFP fusion allowed us to monitor subcellular localization of this protein with fluorescent microscopy. Dissimilar to overproduced YFP, which showed the expected diffuse fluorescence (Fig 1, right) and served as a negative control for protein aggregation, overproduced Sch9-YFP formed distinct fluorescent foci, either one or multiple foci per cell (Fig 1, left). We wondered what can determine the fluorescence pattern in particular cells. Importantly, diversity of fluorescent patterns in BY4742 and *sch9Δ*-BY4741 strains was very similar (Fig 1), and

for subsequent experiments we preferentially used the *SCH9* strain (BY4742) because of its higher growth rate.

The Sch9 protein was listed in several screens for potentially amyloidogenic proteins [25, 26]; however, its amyloidogenic properties have not been closely examined. We hypothesized that fluorescent foci visible in the cells may correspond to amyloid aggregates. To check this hypothesis, we performed an SDD-AGE analysis, a method routinely used for analysis of detergent-resistant aggregates [27], and found that overproduced Sch9-YFP indeed formed detergent-resistant aggregates, which dissolved upon boiling with SDS (Fig 2A). This result was further confirmed with SDS-PAGE: only minor fraction of Sch9 was present on lanes with unboiled samples (Fig 2B).

Different Sch9 domains determine the pattern of its aggregation

Sch9 is enriched with asparagine residues. This feature is typical for yeast aggregation-prone proteins. To determine specific region(s) that might be responsible for aggregation, we chose ArchCandy [28] among several available software tools for amyloidogenicity prediction [29]. Among a variety of different analogs we chose this due to accumulating evidence of its accuracy [28, 30, 31]. This analysis returned several regions in the N-terminal part of the protein (Fig 2C). At the same time, the kinase domains are located in the C-terminal part of the protein. Finally, there are two distinct C2 domains (Fig 2C), which are responsible for membrane binding [32].

We made several deletion constructs removing: the potentially amyloidogenic region with the highest cumulative ArchCandy score (Δ183-256), all regions predicted by ArchCandy (Δ91-138Δ183-256), the N-terminal of the protein until the end of the last of these regions (Δ2-250), the N-terminal part of the protein up to the beginning of the protein kinase domain (Δ2-402), and a reciprocal construct lacking the kinase domains (Δ403-824) (Fig 2D). Each construct was checked with sequencing and SDS-PAGE with Western blotting for production of proteins of expected weights (S2A Fig). Then we tested aggregation with simultaneous analysis with SDD-AGE and SDS-PAGE. In each case, the proteins aggregated, even though in the case of Δ403-824 we could not detect signal on SDD-AGE (Fig 2E, S2B Fig), probably because of low amount of the target protein in cell lysates as judged by SDS-PAGE results (S2B Fig).

Interestingly, even the construct with the longest N-terminal stretch deleted (Δ2-402) formed aggregates indistinguishable from those formed by the full-length protein (Fig 2A, S2B Fig). As both this construct (Δ2-402) and the reciprocal deletion construct (Δ403-824) formed aggregates, as well as all other truncated variants of Sch9, we conclude that this protein contains multiple determinants of aggregation. Nevertheless, we observed changes in aggregates morphology upon overexpression of different constructs. Lack of amino acids 2-250 preserved formation of small foci, while the absence of region 183-256, and potentially 91-38, led to amorphous shape of big aggregates, which are almost spheric in case of wild type.

The formation of foci is not connected with the [*PIN*$^+$] prion, the IPOD compartment or vacuole. As we observed a number of fluorescent phenotypes (cells with different combinations of large and small dots), we wondered what could determine the observed intracellular location of Sch9 and its aggregation.

First, we posed a question whether Sch9-YFP interacts with the Rnq1 amyloid aggregates. The prion form of the Rnq1 protein, the [*PIN*$^+$] (or [*RNQ*$^+$]), is present in many wild and laboratory strains [33, 34], particularly in the BY4741 strain [35], which is closely related to the BY4742 strain we used [36]. We obtained a [*pin*$^-$] derivative of the BY4742 strain by passaging the strain on guanidinium chloride-containing medium [35]. The different [*PIN*$^+$] status of

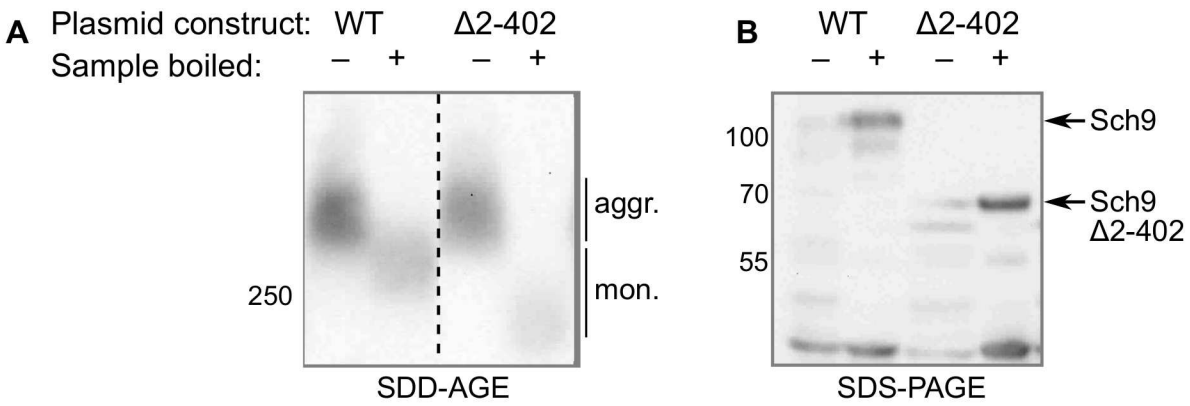

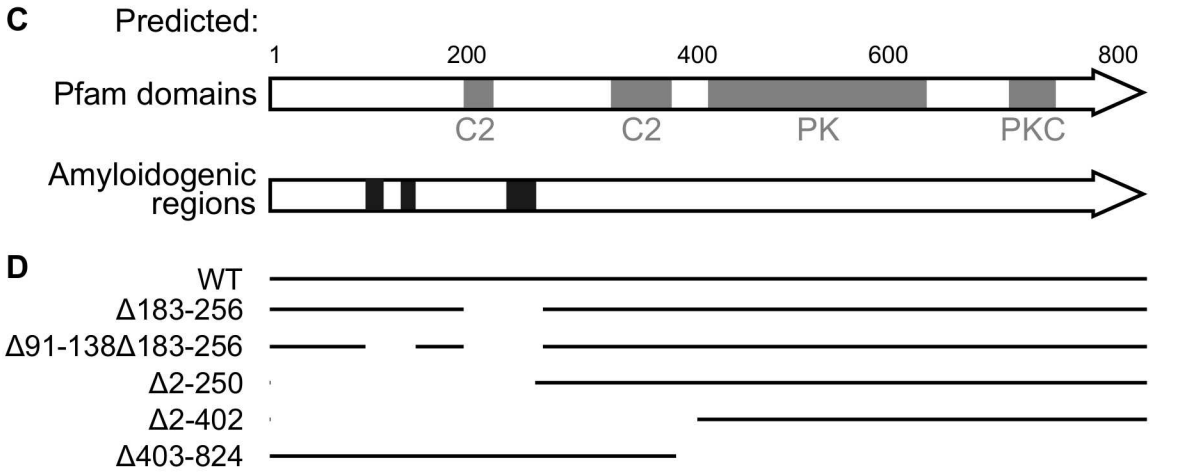

E

Plasmid construct:	Aggregation detected with the following method: Microscopy	SDD-AGE	SDS-PAGE
WT	+	+	+
Δ183-256	+	+	+
Δ91-138Δ183-256	+	+	+
Δ2-250	+	+	+
Δ2-402	+	+	+
Δ403-824	+	ND	+

Fig 2. Overproduced Sch9-YFP forms SDS-resistant aggregates. A: Western blotting after SDD-AGE analysis of representative constructs (shown below). Anti-(CGY)FP antibody was used. B: Western blotting after SDS-PAGE analysis. The same lysates as in A were used. Anti-732-743-Sch9-antibody was used. Dashed line separates different lanes from the same blot. Numbers to the left of blots correspond to the molecular weights (kDa) of protein ladder. aggr., aggregated fraction; mon., monomeric fraction. C: Schematic of the Sch9 domain structure according to the *Saccharomyces* genome database (https://www.yeastgenome.org/locus/S000001248) and amyloidogenic regions were predicted using ArchCandy [28] (see Materials and methods for details). PK, protein kinase domain; PKC, protein kinase C domain; C2, domain involved in membrane contact. D: Sch9 deletion constructs used in this work. E: Summary of amyloidogenicity checks for the deletion constructs shown in (C). For detail see S2 Fig.

https://doi.org/10.1371/journal.pone.0193726.g002

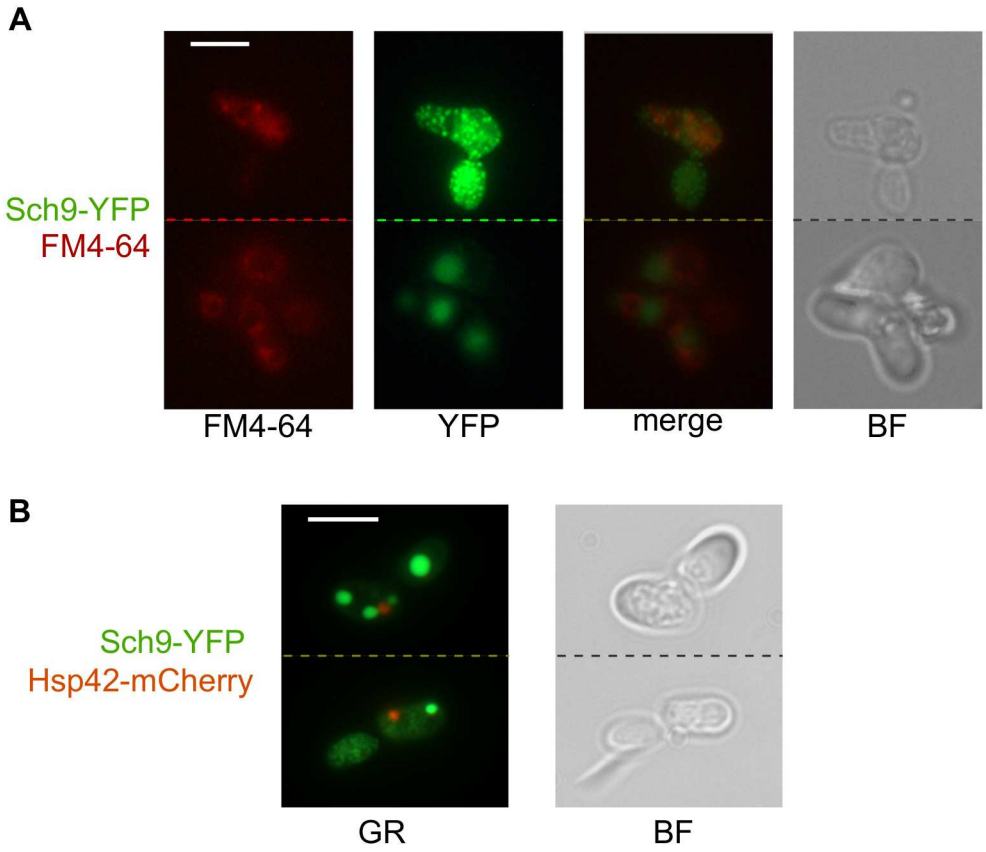

Fig 3. Large Sch9-YFP foci colocalize with neither vacuolar membranes nor IPOD. A: Vacuolar membranes were stained with FM4-64, and these images were merged computationally to study relative location of the stained vacuolar membranes and YFP. B: Co-localization of the Sch9-YFP and Hsp42-mCherry constructs were visualized with the 74 HE GFP+mRFP shift free filter (GR) to observe both proteins at the same time. The scale bar corresponds to 5 μm. BF, bright-field microscopy. Dashed lines separated different fields of view.

https://doi.org/10.1371/journal.pone.0193726.g003

each strain was verified by decoration of the [*PIN*$^+$] aggregates with Rnq1-GFP (S3 Fig, upper row). The [*PIN*$^+$] and [*pin*$^-$] strains showed similar Sch9-YFP fluorescence patterns (S3 Fig, lower row). At least 250 cells for each condition were quantified, and the distributions of cells with different fluorescent patterns were not significantly different (data not shown). Thus, we conclude that the aggregation of Sch9-YFP is independent of [*PIN*$^+$].

Second, Sch9 is known to at least partially reside in the vacuolar membrane [2, 37]. To test whether Sch9-YFP foci might correspond to vacuoles, we used FM4-64, or SynaptoRed C2, to stain vacuolar membranes, and did not see clear colocalization; instead, Sch9-YFP foci were visualized close to the vacuole, but not inside this organelle (Fig 3A). So, our data strongly suggest that even if some of the Sch9-YFP fusion protein is localized in the vacuolar membrane, this fact cannot explain the fluorescence patterns.

Finally, many aggregation-prone proteins are stored in the IPOD compartment localized near the vacuole [38]. Using co-overproduction of Sch9-YFP and Hsp42-mCherry (a marker of IPOD [39]), we checked whether large Sch9-YFP foci might correspond to IPOD. This hypothesis also proved wrong, as in absolute majority (99 out of 100 cells analyzed) Hsp42-mCherry and Sch9-YFP foci did not overlap. A typical example is shown at Fig 3B.

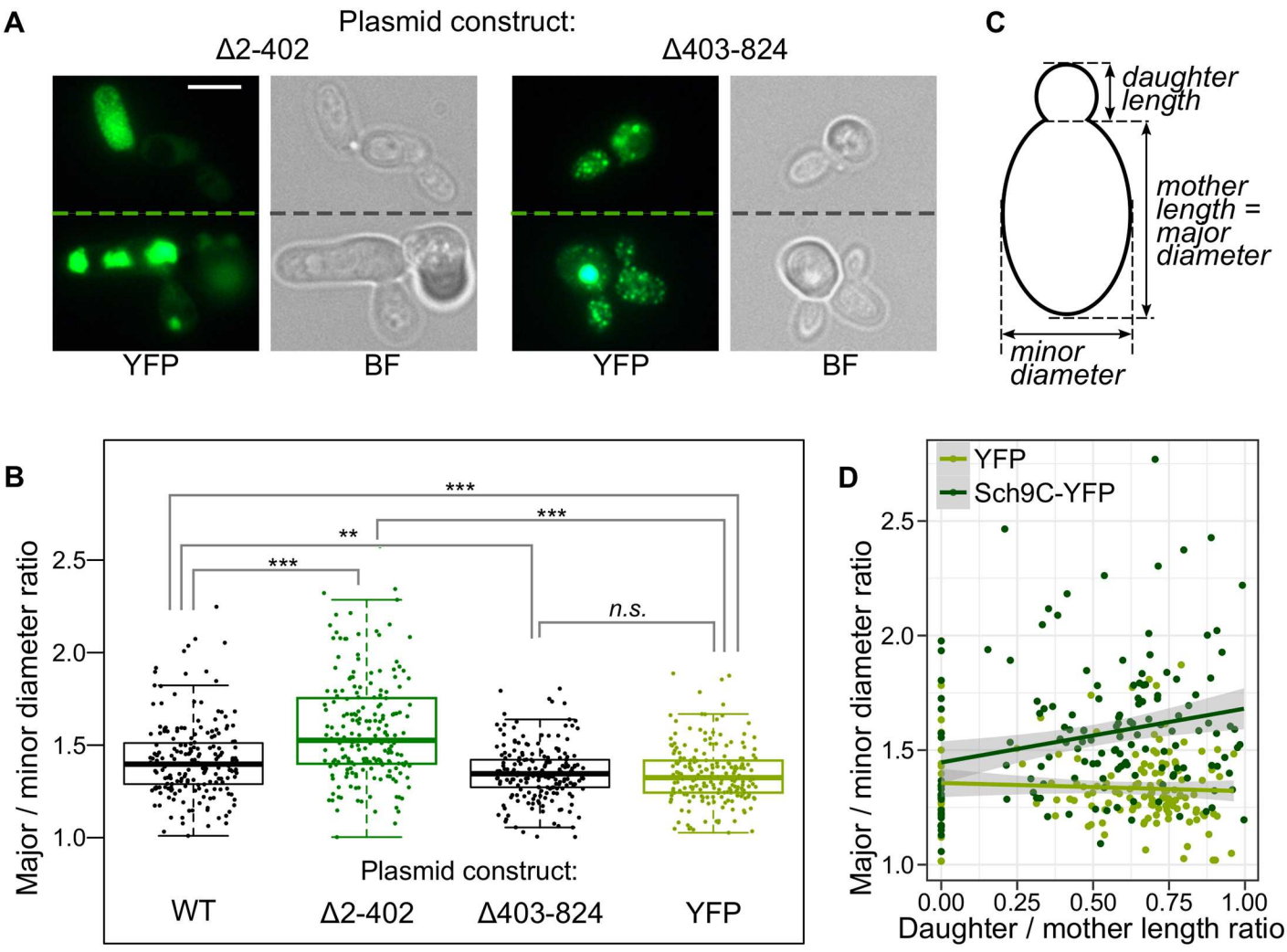

Fig 4. The C- and N-terminal regions of the Sch9 proteins play different roles in its aggregation and phenotype. A: Representative microphotographs of cells overproducing the indicated constructs. Dashed lines separated different fields of view. The scale bar corresponds to 5 μm. BF, bright-field microscopy. B: Box plot summarizing major / minor cell diameter ratios of 200 cells with each construct shown below the graph. Each dot corresponds to individual cell, the central line is the median, box edges show the interquartile range, and whisker length correspond to maximum or minimal values within 1.5 interquartile ranges up and down from the box. **, $p < 0.01$; ***, $p < 0.001$; *n.s.*, $p > 0.05$. Mann-Whitney test with Holm correction was used. C: Schematic of measurements producing values in panels B and D. D: Scatterplot visualizing the relationship between relative bud length and major / minor mother diameter ratio (the vertical axis is the same as in panel B). The line shows predicted values according to a linear regression model; 95% confidence intervals are shown. Bud size, which was determined as the ratio of lengths of daughter and mother cells and, can be used to roughly estimate cell cycle stage [40].

https://doi.org/10.1371/journal.pone.0193726.g004

Overproduction of Sch9 leads to cell elongation, and the C-terminal part of the protein is responsible for this effect

We noticed that BY4742 cells overproducing Sch9-YFP were elongated (Fig 1). To find out which region of the protein was responsible for this effect, we compared form of the cells overproducing either the N-terminal or the C-terminal halves of the protein and found that the cells overproducing the C-terminal region (Sch9Δ2-402) were elongated, while those overproducing the N-terminal region (Sch9Δ403-824) were not (Fig 4A). Interestingly, the fluorescent phenotypes of cells overproducing these constructs were also different: while the C-terminal part of the protein formed either very small dots or large dots (the latter often had irregular shape), the N-terminal part mostly formed clearly visible round dots of varying size (Fig 4A).

The elongation of cells seemed even more prominent in the case of the C-terminal part (Δ2-402) than in the case of the full-length protein (WT) (Fig 4A *cf.* Fig 1). To test this effect statistically, we quantified the ratio of major and minor ellipse diameters (Fig 4C) of at least 200 cells overproducing either Sch9-YFP, Sch9Δ2-402-YFP, Sch9Δ403-824-YFP or the YFP control. Indeed, the C-terminal construct led to the most prominent cell elongation (the highest major/minor diameter ratio), while the cells overproducing the Sch9Δ403-824-YFP construct were indistinguishable from the control ones overproducing YFP (Fig 4B). Thus, cell elongation upon Sch9 overproduction is mediated by the C-terminal part of the protein, which contains its kinase domains.

To find out whether this effect was TOR-dependent, we treated the cells with rapamycin, an antibiotic blocking TORC1 [41]. This treatment led to rounding of cells and abolished the effect of Sch9-YFP, as cells overproducing YFP and Sch9-YFP looked similar (S4A Fig). Thus, the cell elongation we observed upon Sch9 overproduction might be TOR-dependent, as it was dominated by the effect of rapamycin treatment.

To further delve into the mechanism behind cell elongation, we measured bud sizes for the cells and explored the relationship between relative bud size and cell elongation. Relative bud size, which can be used as a parameter characterizing the position of the cell in the cell cycle [40], was determined as the ratio of major diameters of the daughter and mother cells (Fig 4C). This analysis was performed for the control construct (YFP) and the Sch9 allele that had the most pronounced effect (Sch9Δ2-402-YFP). While in the control cell population cell shape (ratio of major/minor diameters of the cell) does not depend on bud size (slope = -0.04, $p = 0.46$; Fig 4D), when Sch9Δ2-402-YFP is overproduced, cell elongation and bud size have a clear positive relationship (slope = 0.24, $p = 0.003$; Fig 4D). Then we performed the same analysis for YFP overproduction *vs.* an empty vector control and found no difference (S4B and S4C Fig). In addition, we compared distributions of cells with different bud sizes between Sch9Δ2-402-YFP overproduction and control (YFP overproduction) and found that the distributions were different ($p = 0.0009$ in Kolmogorov-Smirnov test) with more cells with large buds in the case of Sch9-Δ2-402-YFP overproduction. So, cell elongation caused by Sch9 overproduction is correlated with bud size.

Discussion

In this work, we show that the Sch9 protein forms detergent-resistant (*i.e.*, amyloid-like) aggregates upon overproduction in yeast cells (Fig 2, S2 Fig). Intriguingly, it seems that both the N-terminal and the C-terminal halves of the protein contain some determinants of aggregation, even though aggregation-prone regions were predicted only in the N-terminal part. This is the distinctive feature of Sch9 because in most cases aggregation-prone region and functional domain do not overlap [42]. Nevertheless, at least one protein (Rnq1) with multiple regions responsible for aggregation was described earlier [43]. Since the C-terminal part of the protein contains conservative kinase domains [24], our data on Sch9 aggregation might turn out to be relevant for similar proteins in other organisms. Thus, it might be important to consider possibility of protein aggregation when studying the mammalian AGC kinases, which are sometimes overproduced in cancers.

The aggregation of Sch9 probably causes its accumulation in large intracellular structures, which we in our system visualize as fluorescent foci. All constructs formed aggregates resistant to cold SDS treatment, as revealed by protein analysis with Western blotting (Fig 2A and 2B and S2B Fig). However, not in all cases aggregates could be visualized with SDD-AGE, probably because of low protein level in the case of constructs lacking the longest N-terminal protein stretches, namely Δ2-250 and Δ2-402 (S2B Fig, SDS-PAGE). As these short proteins were

produced at high level, as checked with a fast method of protein extraction based on alkaline lysis (S2A Fig), we suggest that the N-terminal region of the protein is important for its stability. We faced the same problem when trying to analyze aggregation of full length untagged Sch9 encoded by the chromosomal *SCH9* copy. The protein could be detected by Western blotting only if alkaline lysis procedure was used to prepare the sample. Unfortunately, this method of protein extraction requires boiling in SDS and thus does not allow analysis of detergent resistant aggregates in the probe. Thus, we could not directly check whether the wild-type Sch9 forms aggregates. Nevertheless, we suppose that the untagged protein also can aggregate, as there are no obvious limitations. The problem of low-copy Sch9 visualization also did not allow us to check if its aggregates possess prion-like properties, *i.e.*, are self-propagated even after the end of overproduction. This question is very interesting especially in the light of a recent work that revealed that overproduction of different yeast proteins leads to appearance of new phenotypic traits [44]. Thus, from this point of view it is very important to investigate changes of the level of Sch9 upon different treatments. So far, it has been shown that at least carbon source may affect this parameter [2].

Interestingly, for almost all constructs, we noted within-clone variability of fluorescent phenotypes, from multiple small dots to one large dot with possible combinations in between (Fig 1, S2C Fig and Fig 4A). As we could not sort cells prior to protein extraction, we cannot determine which type or types of foci corresponds to detergent resistant aggregates. However, lack of some regions led to visible changes in shape of fluorescent foci. We noticed that constructs lacking one or both C2 domains, which are important for protein-lipid interaction [32], tend to form aggregates of irregular shape (S2C Fig). This result could suggests a link between Sch9 aggregation and its location in the vacuolar membrane, but we did not see colocalization even between round aggregates vacuolar membrane (Fig 3A). Furthermore, these aggregates did not also correspond to IPOD, the structure in which many aggregation-prone proteins are stored in the yeast cell (Fig 3B); thus, we could not identify the subcellular compartment, in which these aggregates are located. It might be possible that overproduced Sch9 forms a specific intracellular structure.

Formation of protein aggregates or phase separated particles may be implicated into different processes [45, 46]. Such examples have been accumulating extensively during past decade. Although the first examples were basically described as different kinds of misfolded protein deposits [47], recent findings demonstrate more and more complicated functions of such complexes. For instance, aggregation of the Whi3 protein in yeast cells acts as a mnemon and changes cellular behavior [48]). In addition, a set of constitutive and likely functional yeast amyloids has been replenished by new examples [49]. Moreover, activation of T cell receptors has been recently shown to lead to formation of liquid droplets enriched by kinases in a model system. These complexes promote actin filament assembly [50]. Following these numerous examples, we can speculate that Sch9 complexes also are implicated in some regulatory processes.

We also found a phenotype connected with *SCH9* overexpression, elongation of cells. Interestingly, even though large cell phenotype was shown for *SCH9* overexpression [2], changes in cell shape, to the extent of our knowledge, has not been reported yet. This difference might be explained by the fact that we exploited a system with high-level constitutive overexpression driven by the *GPD* (*TDH3*) promoter. Here we showed that Sch9-YFP overproduction led to cell elongation, and this effect was more pronounced for cells with larger buds (Fig 4D). We also noted that Sch9-YFP overproduction slowed growth rate (S1D Fig). Taken together, these results suggest that cell elongation caused by Sch9 overproduction is correlated with mitotic delay.

Cell elongation was likely strain specific, as this effect was observed in BY4742 cells but was not so prominent in *sch9Δ*-BY4741 cells (Fig 1). These two strains are closely related and should differ by only a handful of genetic markers: mating type, *LYS2* and *MET15* alleles and of course the presence of *SCH9*. However, the feature determining this phenotypic effect is not either, as there are other BY4741-based strains that react to Sch9 overproduction with clearly seen elongation and at least one *SCH9* strain not closely related to S288C that does not elongate in response to Sch9 overproduction (data not shown). Thus, the mechanism underlying strain specificity of this trait is still to be uncovered.

Our findings for the first time demonstrate the ability of the Sch9 protein to form specific intracellular structures, at least some of which possess amyloid-like properties. In addition, here we attempt to separately analyze functions of the different Sch9 domains and reveal specific effect of the C-terminal region overproduction on cell elongation and existing of several aggregation-prone regions in different parts of the protein. Even though this analysis may be considered as incomplete, we believe that the obtained results complement prior knowledge about Sch9 functions and create a basis for further investigation. Finally, the constructs we present can be exploited to create superior yeast-based model systems to study processes behind AGC kinase overproduction in cancers. These potential model systems could also be useful for testing novel inhibitors of AGC kinases, for example p70S6K, inhibitors of which are already being developed [51–53].

Materials and methods

Microbial strains and cultivation procedures

Throughout this work, two S288C-related *S. cerevisiae* strains were used: an *sch9Δ* strain JW 03 038 BY4741 (genotype *MAT*a *his3Δ1 leu2Δ0 met15Δ0 ura3Δ0 sch9Δ::NATMX4* [9, 54]), which is also referred to in the text as *sch9Δ*-BY4741, and *SCH9* strain BY4742 (*MATα his3Δ1 leu2Δ0 lys2Δ0 ura3Δ0* [36]).

Escherichia coli strain DH5α [55] was used for plasmid selection, maintenance and amplification. Standard yeast and bacterial media with minor modifications were used [56, 57]. The Gal/Raff medium contained 2% galactose and 1% raffinose instead of glucose. For curing of the [*PIN*$^+$] prion, guanidinium chloride was added into the YEPD medium in the final concentration of 5 mM, and cells were passaged three times. Rapamycin treatment was performed with 100 nM rapamycin in liquid SC-Ura medium for 2 hours. Yeast strains were grown at 30 ˚C and the *E. coli* strain was grown at 37 ˚C.

Plasmid construction

Plasmids used in this work and primers used for their construction are listed in S1 and S2 Tables, respectively. Cloning was performed in accordance with standard protocols [57].

To construct p426GPD-SCH9YFP, the *SCH9* ORF without the stop codon was amplified with primers Sch9-F-SpeI and Sch9-R-BamHI and inserted into BamHI/SpeI cut p426GPDSWI1YFP [58]. p426GPD-YFP was constructed by blunting the ends of BamHI/SpeI cut p426GPDSWI1YFP with Klenow fragment and subsequent ligation. p426GPD-SCH9Δ183-256-YFP was made with NheI/XmaJI restriction of p426GPD-SCH9YFP and subsequent vector self-ligation. 426GPD-SCH9Δ2-250-YFP was made from p426GPD-SCH9YFP via obtaining long PCR product and recombination in bacteria [59]. The same method was applied to obtain p426GPD-SCH9Δ91-138Δ183-256-YFP, but in this case p426GPD-SCH9Δ183-256-YFP was used as a template. p426GPD-SCH9Δ2-403-YFP and p426GPD-SCH9Δ403-824-YFP were constructed by replacing the full length *SCH9* with its shorter alleles (obtained as PCR products with the same template) at SpeI/BamHI sites.

pRS416-SCH9YFP was constructed by subcloning the XmaJI/KpnI restriction fragment of p426GPD-SCH9YFP into pJU675 [1]. All constructs were verified with restriction digest and insert sequencing. Plasmid maps are available in S1 Maps.

pRS415CUP-RNQ1GFP (Derkatch, unpublished) was used to monitor the [*PIN*$^+$] status of the strain, and pAG415GPD-Hsp42-mCherry [39] was used to locate IPOD. pRS416 [60] and pRS426 [61] were used as empty vector controls. Maps of pRS plasmids were modified according to the published corrections [62].

Microscopy

Staining with FM4-64 (Invitrogen) was performed according to the published protocol [63] with slight modifications: YEPD was used instead of YES, and cells were grown for 120 minutes after washing off non-bound dye. Cells producing YFP or mCherry fusion proteins were grown in synthetic media until late logarithmic phase (cell density about 10^7 cells/ml), mixed with glycerol (25% final concentration) and observed with Zeiss Axio Scope.A1. The following filters were used: 46 (excitation peak 500 nm / emission peak 535 nm) for Sch9-YFP fusions, 63 HE mRFP shift free (excitation peak 572 nm / emission peak 629 nm) for the Hsp42-mCherry fusion and FM4-64, 74HE GFP+mRFP shift free for detection of autofluorescence or simultaneous detection of YFP and mCherry (excitation peaks 483 and 569 nm / emission peaks 636 nm). Shooting exposure was chosen empirically for informativeness and may not necessarily be the same for different constructs.

Biochemical methods

For protein extraction, cells were grown in synthetic media until late logarithmic phase (cell density about 10^7 cells/ml) and collected with centrifugation (about 10^7 cells for alkaline lysis [64] or about 2×10^8 cells for mechanical cell disruption [65]). As alkaline lysis allows to achieve higher protein concentration [64] and reduced degradation (compare S2A and S2B Fig), but due to the procedure requires sample boiling, it was used to check protein production, while mechanical cell disruption was used to assess protein aggregation.

SDS-PAGE [57] or SDD-AGE [27] was used for separation of the proteins, and PVDF membranes (GE Healthcare) were used for semi-dry [57] or capillary transfer [66], respectively. Blots were probed with either anti-732-743-Sch9 and anti-phospho-Thr737-Sch9 [67] or anti-Tag(CGY)FP (Evrogen AB121) antibodies and photographed with GeneGnome (SynGene).

Data analysis

The ArchCandy [28] program was used for prediction of amyloidogenic regions (0.575 was used as threshold value without any additional built-in filters). Following the recommendation of the developers, we considered only those β-arches that were located in unstructured regions. The IUPred program [68] with *long* option was used for prediction of such regions, the recommended threshold 0.5 was used.

ImageJ [69] was used for measuring major and minor axes of cells with the *fit ellipse* measurement option. Custom R [70] scripts were also used for data analysis. The Mann-Whitney U test implemented in the coin package [71] was used to test differences in ellipse axis ratio. Distribution of cells with buds of different sizes were compared with the ks.test function, and linear regression models were built with the lm function of the base R package [70]. The ggplot2 package [72] was used to plot scatterplots with regression lines and 95% confidence intervals.

Supporting information

S1 Fig. Sch9-YFP is functional and not toxic when overproduced. A: Western blot probed with anti-732-743-Sch9 antibody. B: Western blots probed with anti-732-743-Sch9 or anti-phospho-Thr737-Sch9 antibody. The same lysates were loaded into both gels. Approximate molecular weight in kDa is shown according to a standard protein weight ladder. C: Five-fold serial dilutions of the respective transformants. A-C: *WT* and *Δ* designate BY4742 and *sch9Δ*-BY4741 strains, respectively. Dashed lines mark additional lanes removed for clarity. SCH9-YFP, p426GPD-SCH9YFP; YFP, p426GPD-YFP. D: Five-fold serial dilutions of representative transformants of the *sch9Δ*-BY4741 strain. Plasmids used (from left to right): pRS416, pJU675, pRS416-SCH9YFP, p426GPD-YFP, p426GPD-SCH9YFP. C-D: Cell concentration decreases from top to bottom.
(TIF)

S2 Fig. Representative examples of results of the amyloidogenicity analysis of different Sch9 deletion constructs. A: Western blotting of membranes with boiled cell lysates obtained with alkaline lysis and separated with SDS-PAGE. The primary antibodies used for probing are shown under each blot. B: Results of fluorescent microscopy, SDD-AGE and SDS-PAGE analysis of cells overproducing each Sch9 construct (shown in the leftmost column). Dashed lines separated different fields of view chosen from the same slide or different lanes from the same blot. Lysates of cells overproducing the full-length protein (WT) are shown for comparison on each blot image. The plus and minus signs indicate whether the sample was boiled. Scale bars on microphotographs correspond to 5 μm. Numbers to the left of blots show the position of the corresponding protein molecular weight standard (kDa).
(TIF)

S3 Fig. Sch9-YFP fluorescent patterns are independent of the [*PIN*$^+$] prion status. Dashed lines separated different fields of view chosen from the same slide. The scale bar corresponds to 5 μm. BF, bright-field microscopy. For Rnq1-GFP overproduction, $CuSO_4$ was added to the final concentration of 50 μM, and then cells were incubated for 3 hours.
(TIF)

S4 Fig. YFP overproduction does not affect cell shape, while rapamycin treatment overcomes the effect of Sch9-YFP overproduction. A: Microphotographs of cells treated with rapamycin. Dashed lines separated different fields of view from the same slide. The scale bar indicates 8 μm. B: Box plot summarizing major / minor cell diameter ratios of at least 90 cells with each construct shown below the graph. Each dot corresponds to individual cell, the central line is the median, box edges show the interquartile range, and whisker length correspond to maximum or minimal values within 1.5 interquartile ranges up and down from the box. *n.s.*, $p > 0.05$ in Mann-Whitney test. C: Scatterplot visualizing the relationship between relative bud length and major / minor mother diameter ratio.
(TIF)

S1 Table. List of plasmids used in this work. The description column lists the characteristics in the following order: *S. cerevisiae* replication origin, *S. cerevisiae* selective marker gene, *E. coli* selective marker gene, promoter, and gene of interest.
(XLS)

S2 Table. List of primers used in this work.
(XLS)

S1 Maps. Maps of the plasmids constructed in this work and other plasmids used (if available).
(ZIP)

Acknowledgments

The authors are grateful for Maria Cordenaz-Corona and Joanne Kingsbury for their generous gift of anti-732-743-Sch9 and anti-phospho-Thr737-Sch9 antibodies, Simon Alberti for the pAG415GPD-Hsp42-mCherry plasmid, Tobias Wilms for the JW 03 038 strain, Jörg Urban for the pJU675 plasmid and Aleksandr Rubel for the FM4-64 dye. We would like to thank Andrew Matveenko for useful advice and help with plasmid construction. The research was supported by the research resource center "Molecular and cell technologies" of the St. Petersburg State University.

Author Contributions

Conceptualization: Polina Drozdova, Galina Zhouravleva, Stanislav Bondarev.

Funding acquisition: Galina Zhouravleva, Stanislav Bondarev.

Investigation: Polina Drozdova, Polina Lipaeva, Tatyana Rogoza, Stanislav Bondarev.

Methodology: Polina Drozdova, Polina Lipaeva, Tatyana Rogoza, Stanislav Bondarev.

Project administration: Galina Zhouravleva.

Supervision: Polina Drozdova, Stanislav Bondarev.

Visualization: Polina Drozdova, Stanislav Bondarev.

Writing – original draft: Polina Drozdova.

Writing – review & editing: Polina Drozdova, Tatyana Rogoza, Galina Zhouravleva, Stanislav Bondarev.

References

1. Urban J, Soulard A, Huber A, Lippman S, Mukhopadhyay D, Deloche O, et al. Sch9 is a major target of TORC1 in *Saccharomyces cerevisiae*. Mol Cell. 2007; 26: 663–74. https://doi.org/10.1016/j.molcel.2007.04.020 PMID: 17560372
2. Jorgensen P, Rupes I, Sharom JR, Schneper L, Broach JR, Tyers M. A dynamic transcriptional network communicates growth potential to ribosome synthesis and critical cell size. Genes Dev. 2004; 18: 2491–505. https://doi.org/10.1101/gad.1228804 PMID: 15466158
3. Fabrizio P, Pozza F, Pletcher SD, Gendron CM, Longo VD. Regulation of longevity and stress resistance by Sch9 in yeast. Science. 2001; 292: 288–90. https://doi.org/10.1126/science.1059497 PMID: 11292860
4. Lu YJ, Swamy KBS, Leu JY. Experimental evolution reveals interplay between Sch9 and polyploid stability in yeast. Murray AW, editor. PLoS Genet. Public Library of Science; 2016; 12: e1006409. https://doi.org/10.1371/journal.pgen.1006409
5. Jorgensen P, Nishikawa JL, Breitkreutz B-J, Tyers M. Systematic identification of pathways that couple cell growth and division in yeast. Science. 2002; 297: 395–400. https://doi.org/10.1126/science.1070850 PMID: 12089449
6. Kaeberlein M, Powers RW, Steffen KK, Westman EA, Hu D, Dang N, et al. Regulation of yeast replicative life span by TOR and Sch9 in response to nutrients. Science. American Association for the Advancement of Science; 2005; 310: 1193–6. https://doi.org/10.1126/science.1115535
7. Weinberger M, Feng L, Paul A, Smith DL, Hontz RD, Smith JS, et al. DNA replication stress is a determinant of chronological lifespan in budding yeast. Bielinsky A-K, editor. PLoS One. Public Library of Science; 2007; 2: e748. https://doi.org/10.1371/journal.pone.0000748

8. Madia F, Wei M, Yuan V, Hu J, Gattazzo C, Pham P, et al. Oncogene homologue Sch9 promotes age-dependent mutations by a superoxide and Rev1/Polζ-dependent mechanism. J Cell Biol. 2009; 186: 509–523. https://doi.org/10.1083/jcb.200906011 PMID: 19687253
9. Swinnen E, Wilms T, Idkowiak-Baldys J, Smets B, De Snijder P, Accardo S, et al. The protein kinase Sch9 is a key regulator of sphingolipid metabolism in *Saccharomyces cerevisiae*. Mol Biol Cell. American Society for Cell Biology; 2014; 25: 196–211. https://doi.org/10.1091/mbc.E13-06-0340
10. Hunter T, Plowman GD. The protein kinases of budding yeast: six score and more. Trends Biochem. Sci. 1997; 22: 18–22.
11. Arencibia JM, Pastor-Flores D, Bauer AF, Schulze JO, Biondi RM. AGC protein kinases: from structural mechanism of regulation to allosteric drug development for the treatment of human diseases. Biochim Biophys Acta. 2013; 1834(7): 1302–21. https://doi.org/10.1016/j.bbapap.2013.03.010 PMID: 23524293
12. Van Dam TJP, Zwartkruis FJT, Bos JL, Snel B. Evolution of the TOR pathway. J Mol Evol. 2011; 73: 209–220. https://doi.org/10.1007/s00239-011-9469-9 PMID: 22057117
13. Arul N, Cho YY. A Rising Cancer Prevention Target of RSK2 in Human Skin Cancer. Front Oncol. 2013 Aug 5; 3:201. https://doi.org/10.3389/fonc.2013.00201 PMID: 23936765
14. Madhunapantula SV, Robertson GP. Therapeutic implications of targeting AKT signaling in melanoma. Enzyme Res. 2011 Mar 23; 2011:327923. https://doi.org/10.4061/2011/327923 PMID: 21461351
15. Fagerli U-M, Ullrich K, Stuhmer T, Holien T, Kochert K, Holt Ru, et al. Serum/glucocorticoid-regulated kinase 1 (SGK1) is a prominent target gene of the transcriptional response to cytokines in multiple myeloma and supports the growth of myeloma cells. Oncogene. 2011; 30:3198–3206. https://doi.org/10.1038/onc.2011.79 PMID: 21478911
16. Hoang B, Shi Y, Frost PJ, Mysore V, Bardeleben C, Lichtenstein A. SGK kinase activity in multiple myeloma cells protects against ER stress apoptosis via a SEK-dependent mechanism. Mol Cancer Res. 2016 Apr; 14(4):397–407. https://doi.org/10.1158/1541-7786.MCR-15-0422 PMID: 26869290
17. Pardo OE, Seckl MJ. S6K2: The neglected S6 kinase family member. Front Oncol. 2013 3:191. https://doi.org/10.3389/fonc.2013.00191 PMID: 23898460
18. Tavares MR, Pavan IC, Amaral CL, Meneguello L, Luchessi AD, Simabuco FM. The S6K protein family in health and disease. Life Sci. 2015; 131:1–10. https://doi.org/10.1016/j.lfs.2015.03.001 PMID: 25818187
19. Couch FJ, Wang XY, Wu GJ, Qian J, Jenkins RB, James CD. Localization of PS6K to chromosomal region 17q23 and determination of its amplification in breast cancer. Cancer Research. 1999; 59 (7):1408–1411. PMID: 10197603
20. Sinclair CS, Rowley M, Naderi A, Couch FJ. The 17q23 amplicon and breast cancer. Breast Cancer Res Treat. 2003; 78:313–22. https://doi.org/10.1023/A:1023081624133 PMID: 12755490
21. Brugge J, Hung MC, Mills GB. A new mutational AKTivation in the PI3K pathway. Cancer Cell. 2007; 12 (2):104–107. https://doi.org/10.1016/j.ccr.2007.07.014 PMID: 17692802
22. Zhang Y, Martens JW, Yu JX, Jiang J, Sieuwerts AM, Smid M, et al. Copy number alterations that predict metastatic capability of human breast cancer. Cancer Res. 2009; 69:3795–801. https://doi.org/10.1158/0008-5472.CAN-08-4596 PMID: 19336569
23. Perez-Tenorio G, Karlsson E, Waltersson MA, Olsson B, Holmlund B, Nordenskjold B, et al. Clinical potential of the mTOR targets S6K1 and S6K2 in breast cancer. Breast Cancer Res Treat (2011) 128:713–2310. https://doi.org/10.1007/s10549-010-1058-x PMID: 20953835
24. Toda T, Cameron S, Sass P, Wigler M. *SCH9*, a gene of *Saccharomyces cerevisiae* that encodes a protein distinct from, but functionally and structurally related to, cAMP-dependent protein kinase catalytic subunits. Genes Dev. 1988; 2: 517–527. https://doi.org/10.1101/gad.2.5.517 PMID: 3290050
25. Michelitsch MD, Weissman JS. A census of glutamine/asparagine-rich regions: implications for their conserved function and the prediction of novel prions. Proc Natl Acad Sci U S A. 2000; 97: 11910–5. https://doi.org/10.1073/pnas.97.22.11910 PMID: 11050225
26. Harrison PM, Gerstein M. A method to assess compositional bias in biological sequences and its application to prion-like glutamine/asparagine-rich domains in eukaryotic proteomes. Genome Biol. 2003; 4: R40. https://doi.org/10.1186/gb-2003-4-6-r40 PMID: 12801414
27. Kryndushkin DS, Alexandrov IM, Ter-Avanesyan MD, Kushnirov VV. Yeast [*PSI*$^+$] prion aggregates are formed by small Sup35 polymers fragmented by Hsp104. J Biol Chem. 2003; 278: 49636–43. https://doi.org/10.1074/jbc.M307996200 PMID: 14507919
28. Ahmed AB, Znassi N, Château M-T, Kajava AV. A structure-based approach to predict predisposition to amyloidosis. Alzheimer's & Dementia. 2015; 6: 681–690. https://doi.org/10.1016/j.jalz.2014.06.007
29. Ahmed AB, Kajava AV. Breaking the amyloidogenicity code: methods to predict amyloids from amino acid sequence. FEBS letters. 2013; 8: 1089–1095. https://doi.org/10.1016/j.febslet.2012.12.006

30. Bondarev SA, Zhouravleva GA, Belousov MV, Kajava AV. Structure-based view on [*PSI*$^+$] prion properties. Prion. 2015; 3: 190–199. https://doi.org/10.1080/19336896.2015.1044186

31. Roche DB, Villain E, Kajava AV. Usage of a dataset of NMR resolved protein structures to test aggregation *vs*. solubility prediction algorithms. Protein Science. 2017; 26: 1864–1869. https://doi.org/10.1002/pro.3225 PMID: 28685932

32. Corbalan-Garcia S, Gómez-Fernández JC. Signaling through C2 domains: More than one lipid target. Biochimica et Biophysica Acta—Biomembranes. 2014. pp. 1536–1547. https://doi.org/10.1016/j.bbamem.2014.01.008

33. Nakayashiki T, Kurtzman CP, Edskes HK, Wickner RB. Yeast prions [*URE3*] and [*PSI*$^+$] are diseases. Proc Natl Acad Sci U S A. 2005; 102: 10575–10580. https://doi.org/10.1073/pnas.0504882102 PMID: 16024723

34. Halfmann R, Jarosz DF, Jones SK, Chang A, Lancaster AK, Lindquist S. Prions are a common mechanism for phenotypic inheritance in wild yeasts. Nature. 2012; 482: 363–8. https://doi.org/10.1038/nature10875 PMID: 22337056

35. Derkatch IL, Bradley ME, Hong JY, Liebman SW. Prions affect the appearance of other prions: the story of [*PIN*$^+$]. Cell. Elsevier; 2001; 106: 171–82.

36. Brachmann CB, Davies A, Cost GJ, Caputo E, Li J, Hieter P, et al. Designer deletion strains derived from *Saccharomyces cerevisiae* S288C: a useful set of strains and plasmids for PCR-mediated gene disruption and other applications. Yeast. 1998; 14: 115–32. PMID: 9483801

37. Koh JLY, Chong YT, Friesen H, Moses A, Boone C, Andrews BJ, et al. CYCLoPs: A comprehensive database constructed from automated analysis of protein abundance and subcellular localization patterns in *Saccharomyces cerevisiae*. G3 (Bethesda). G3: Genes, Genomes, Genetics; 2015; 5: 1223–1232. https://doi.org/10.1534/g3.115.017830

38. Kaganovich D, Kopito R, Frydman J. Misfolded proteins partition between two distinct quality control compartments. Nature. 2008; 454: 1088–95. https://doi.org/10.1038/nature07195 PMID: 18756251

39. Malinovska L, Kroschwald S, Munder MC, Richter D, Alberti S. Molecular chaperones and stress-inducible protein-sorting factors coordinate the spatiotemporal distribution of protein aggregates. Mol Biol Cell. 2012; 23: 3041–3056. https://doi.org/10.1091/mbc.E12-03-0194 PMID: 22718905

40. Williamson DH. The timing of deoxyribonucleic acid synthesis in the cell cycle of *Saccharomyces cerevisiae*. J Cell Biol. 1965; 25: 517–528. https://doi.org/10.1083/jcb.25.3.517 PMID: 4284570

41. Wullschleger S, Loewith R, Hall MN. TOR signaling in growth and metabolism. Cell. 2006; 10: 471–784. https://doi.org/10.1016/j.cell.2006.01.016

42. Liebman SW, Chernoff YO. Prions in yeast. Genetics. 2012; 191: 1041–72. https://doi.org/10.1534/genetics.111.137760 PMID: 22879407

43. Kadnar ML, Articov G, Derkatch IL. Distinct type of transmission barrier revealed by study of multiple prion determinants of Rnq1. PLoS Genet. 2010; 6: e1000824. https://doi.org/10.1371/journal.pgen.1000824 PMID: 20107602

44. Chakrabortee S, Byers JS, Jones S, Garcia DM, Bhullar B, Chang A, She R, Lee L, Fremin B, Lindquist S, Jarosz DF. Intrinsically disordered proteins drive emergence and inheritance of biological traits. Cell. 2016; 2:369–381.e12. https://doi.org/10.1016/j.cell.2016.09.017

45. Alberti S. The wisdom of crowds: regulating cell function through condensed states of living matter. J Cell Sci. The Company of Biologists Ltd; 2017; 130: 2789–2796.

46. Nizhnikov AA, Antonets KS, Inge-Vechtomov SG. Amyloids: from pathogenesis to function. Biochemistry (Mosc). 2015; 80:1127–1144. https://doi.org/10.1134/S0006297915090047

47. Amen T, Kaganovich D. Dynamic droplets: the role of cytoplasmic inclusions in stress, function, and disease. Cell Mol Life Sci (2015) 72:401–415. https://doi.org/10.1007/s00018-014-1740-y PMID: 25283146

48. Caudron F, Barral Y. A super-assembly of Whi3 encodes memory of deceptive encounters by single cells during yeast courtship. Cell. 2013; 155: 1244–1257. https://doi.org/10.1016/j.cell.2013.10.046 PMID: 24315096

49. Ryzhova TA, Sopova J V., Zadorsky SP, Siniukova VA, Sergeeva A V., Galkina SA, et al. Screening for amyloid proteins in the yeast proteome. Current Genetics. 2017: 1–10.

50. Su X, Ditlev JA, Hui E, Xing W, Banjade S, Okrut J, King DS, Taunton J, Rosen MK, Vale RD. Phase separation of signaling molecules promotes T cell receptor signal transduction. Science. 2016; 352: 595–599. https://doi.org/10.1126/science.aad9964 PMID: 27056844

51. Pearce LR, Alton GR, Richter DT, Kath JC, Lingardo L, Chapman J, et al. Characterization of PF-4708671, a novel and highly specific inhibitor of p70 ribosomal S6 kinase (S6K1) Biochem J. 2010; 431: 245–255. PMID: 20704563

52. Hollebecque A, Houédé N, Cohen EEW, Massard C, Italiano A, Westwood P, et al. A phase Ib trial of LY2584702 tosylate, a p70 S6 inhibitor, in combination with erlotinib or everolimus in patients with solid tumours. Eur J Cancer. 2014; 50: 876–884. https://doi.org/10.1016/j.ejca.2013.12.006 PMID: 24456794

53. Segatto I, Massarut S, Boyle R, Baldassarre G, Walker D, Belletti B. Preclinical validation of a novel compound targeting p70S6 kinase in breast cancer. Aging (Albany NY). 2016; 8(5): 958–76. https://doi.org/10.18632/aging.100954

54. Wilms T, Swinnen E, Eskes E, Dolz-Edo L, Uwineza A, Van Essche R, et al. The yeast protein kinase Sch9 adjusts V-ATPase assembly/disassembly to control pH homeostasis and longevity in response to glucose availability. PLOS Genet. Public Library of Science; 2017; 13: e1006835. https://doi.org/10.1371/journal.pgen.1006835

55. Hanahan D. Techniques for transformation of *E. coli*. In: Glover DM, editor. DNA cloning. Vol. 1. Oxford, United Kingdom: IRL Press; 1985. pp. 109–135.

56. Kaiser C, Michaelis S, Mitchell A. Methods in Yeast Genetics. 1994 Editi. NY: CSHL PRESS; 1994.

57. Maniatis T, Fritsch EF, Sambrook J, others. Molecular cloning: a laboratory manual. Cold Spring Harbor Laboratory Cold Spring Harbor, NY; 1989.

58. Du Z, Park K-W, Yu H, Fan Q, Li L. Newly identified prion linked to the chromatin-remodeling factor Swi1 in *Saccharomyces cerevisiae*. Nat Genet. 2008; 40: 460–465. https://doi.org/10.1038/ng.112 PMID: 18362884

59. Liu H, Naismith JH. An efficient one-step site-directed deletion, insertion, single and multiple-site plasmid mutagenesis protocol. BMC Biotechnol. 2008; 8: 91. https://doi.org/10.1186/1472-6750-8-91 PMID: 19055817

60. Sikorski RS, Hieter P. A system of shuttle vectors and yeast host strains designed for efficient manipulation of DNA in Saccharomyces cerevisiae. Genetics. 1989; 122: 19–27. Available: http://www.genetics.org/content/122/1/19.abstract PMID: 2659436

61. Christianson TW, Sikorski RS, Dante M, Shero JH, Hieter P. Multifunctional yeast high-copy-number shuttle vectors. Gene. 1992; 110: 119–22. Available: https://www.sciencedirect.com/science/article/pii/037811199290454W?via%3Dihub PMID: 1544568

62. Chee MK, Haase SB. New and Redesigned pRS Plasmid shuttle vectors for genetic manipulation of *Saccharomyces cerevisiae*. G3 (Bethesda). G3: Genes, Genomes, Genetics; 2012; 2: 515–26. https://doi.org/10.1534/g3.111.001917

63. Tong Z. Yeast vacuole staining with FM4-64. Bio-protocol Bio101. 2011; e18.

64. Zhang T, Lei J, Yang H, Xu K, Wang R, Zhang Z. An improved method for whole protein extraction from yeast *Saccharomyces cerevisiae*. Yeast. 2011; 28: 795–798. https://doi.org/10.1002/yea.1905 PMID: 21972073

65. Kushnirov VV, Alexandrov IM, Mitkevich OV, Shkundina IS, Ter-Avanesyan MD. Purification and analysis of prion and amyloid aggregates. Methods. 2006; 39: 50–5. https://doi.org/10.1016/j.ymeth.2006.04.007 PMID: 16774835

66. Halfmann R, Lindquist S. Screening for amyloid aggregation by semi-denaturing detergent-agarose gel electrophoresis. J Vis Exp. 2008; 20–22.

67. Kingsbury JM, Sen ND, Maeda T, Heitman J, Cardenas ME. Endolysosomal membrane trafficking complexes drive nutrient-dependent TORC1 signaling to control cell growth in *Saccharomyces cerevisiae*. Genetics. 2014; 196: 1077–1089. https://doi.org/10.1534/genetics.114.161646 PMID: 24514902

68. Dosztányi Z, Csizmók V, Tompa P, Simon I. The pairwise energy content estimated from amino acid composition discriminates between folded and intrinsically unstructured proteins. J. Mol. Biol. 2005; 347: 827–839. https://doi.org/10.1016/j.jmb.2005.01.071 PMID: 15769473

69. Schneider CA, Rasband WS, Eliceiri KW. NIH Image to ImageJ: 25 years of image analysis. Nat Methods. 2012; 9: 671–675. https://doi.org/10.1038/nmeth.2089 PMID: 22930834

70. R Core Team. R: A language and environment for statistical computing. R Foundation for Statistical Computing, Vienna, Austria, 2016.

71. Hothorn T, Hornik K, van de Wiel MA, Zeileis A. Implementing a class of permutation tests: The coin package. J Stat Softw. 2008; 28. Available: http://www.jstatsoft.org/v28/i08/

72. Wickham H. ggplot: Elegant Graphics for Data Analysis. Springer; 2009.